CORPUS PUBLISHERS

Current Trends in Engineering Science (CTES)

ISSN: 2833-356X

Volume 3 Issue 3, 2023

Article Information

Received date : April 13, 2023

Published date: June 19, 2023

*Corresponding author

P Leo, Department of Engineering for Innovation, University of Salento, Italy

DOI: 10.54026/CTES/1034

Keywords

Notch stress concentration; Fatigue failure; Metallographic analysis; Fracture surface

Review Article

On the Mechanical and Metallurgical Causes of an Ultralight Aircraft in-Flight Crash

P Leo*, P Millefiori and R Nobile

Department of Engineering for Innovation, University of Salento, Italy

Abstract

This paper reports the study carried out to define the causes of the in-flight crash of an ultralight aircraft. Two fractured areas were identified after the impact and analysed for that scope. One fracture interested the bolt connecting the engine shaft to the propeller and the second one interested the root of one of the two blade sockets, the other blade was found unbroken. Microstructural and mechanical analysis of samples coming from the bolt and from the blade (respectively CK45 carbon steel and Ni-Cr-Mo steel) do not show any significant metallurgical defects or anomalies. So, the analysis was focused on fractures surfaces of both the bolt and the blade socket. Fatigue crack initiation and propagation at the root of the broken blade socket was identified as the main cause of the failure. The examination of the unbroken blade socket also showed the presence of an extended circumferential crack demonstrating that the stress concentration associated to the notch geometry and the applied stress was critical for the fatigue failure initiation. A deeper investigation about the notch root, also supported by Finite Element Analysis, established that the cause of the failure was the inappropriate value of the radius notch that was lower that the designed one.

Introduction

An ultralight aircraft accident occurred close to Lecce Lepore airport in Italy. Freccia RG-350P is an ultralight two-seater lower wing aircraft having a wing span of 8.78m, total length of 7.25m and maximum weight at take-off of 472.5kg. Propulsion is assured by a two-blade propeller directly connected to an UL350is engine, which allowed reaching a maximum speed of 300 km/h. At the time of the accident, the aircraft had operated for about 16 h. Severe injuries were reported by the two pilots. Aircraft was founded completely destroyed, without the two-blades propeller (Figure 1a). The propeller was founded at about 240 m of distance with only one blade (Figure 1b). The other blade was never found. The propeller was probably lost during the flight due to a mechanical failure, determining the aircraft fall. After the loss of the propeller, the aircraft continued its coasting flight up to the fall. The visual inspection of the propeller highlighted the existence of a surface failure of the bolt connecting the propeller to the driving shaft. The separation of the propeller from the engine shaft is due to the failure of the central bolt, as clearly illustrated by the mounting scheme of figure 2.

Because of the failure, the central bolt body was found screwed to the shaft (Figure 3a), while the hexagonal head was retained by the propeller flange (Figure 3b).

The other relevant failure is located between the blade and the propeller. The blade ends with a screw socket that allows the connection with the blade propeller through an axial bearing. In this case the fracture surface involves different components, including the mechanism used for the tilt regulation of the blade, which is not relevant from a structural point of view (Figure 4).

a b

Figure 1: a) Aircraft Freccia as founded at the impact zone, b) Aspect of the propeller after the crash.

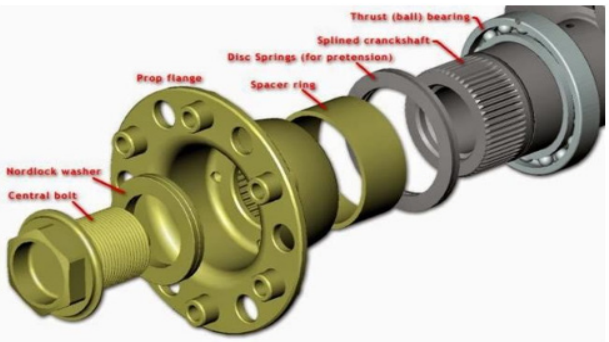

Figure 2: Particular of the mounting of the propeller to the engine shaft.

The procedure followed by the authors to study these two failures was coherent with the practical indication that can be found in several books [1,2]. The authors have first analysed the microstructure and the surface fractures of the failed connection bolt and screw socket, with the aim to identify the materials and to show the existence of material defects responsible for the failure. Then, the visual examination of the unbroken screw socket suggested a possible explanation of the failure and authors validated this hypothesis through a FEM analysis, allowing to successfully identify the causes of the failures and, as a consequence, of the accident. Those temporal sequences of the analysis have been used for presenting the results in the following paragraphs.

The technical analysis allowed to establish that the two failures were not determined by the uncontrolled land impact of the aircraft. Further, the analysis has clarified the accident dynamics, establishing that the primary failure occurred between the blade and the propeller, followed by the failure of the bolt connecting the propeller to the engine shaft.

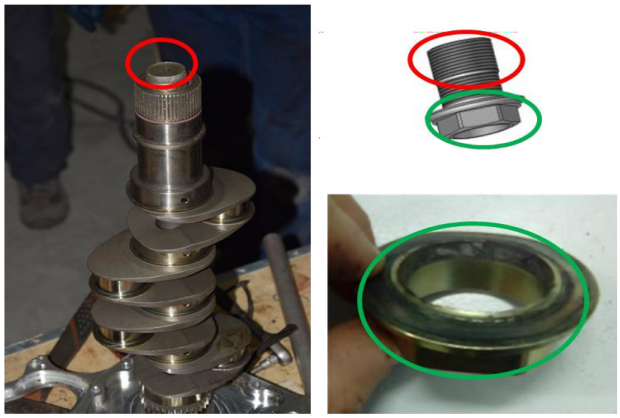

Figure 3: Fracture surface of the central bolt: a) shaft side; b) propeller side.

Figure 4: Aspect of the zone of the defective blade: a) as founded; b) after bearing removal.

Materials and Method

The bolt material is a medium carbon steel designated as CK45. Some of the features of CK45 steel are good machinability, high tensile strength and good impact resistance. It is suitable for rail, axle, and wheel applications [3-6]. CK45 carbon steel is widely used in automotive and engine parts, as well as industrial shafts and rollers [3-8].

The screw socket material is made by 39NiCrMo3 steel. This steel is widely used in heavy-duty components for aeroplanes, general automobile, and technical applications, such as forged propeller shafts, connecting rods, gear shafts, cranks, and landing gear components [3-5,9-10]. The 39NiCrMo3 steel is suitable for different heat treatments and shows a good cold workability [11]. Typically, that steel is quenched and tempered to attain high mechanical properties [3-10,12].

Two samples were cut from the bolt (having a nominal composition of 0.43% C, 0.35% Mn, 0.15% Si, 0.19% Cr, 0.02% Mo, 0.02% P, 0.02% S and Fe %remaining) and the screw socket (having a nominal composition of 0.4% C, 0.8% Cr, 0.2% Mo. 0.9% Ni, 0.3% Si and 0.7% Mn). These samples have been prepared by standard

Metallographic procedures and observed before and after Nital chemical etching (5% Nitric Acid in Etanohol). Optical Microscope (OM) was used for investigating the microstructure while Stereo Microscopy (SM) and Scanning Electron Microscope (SEM) was used for the analysis of the fracture surfaces. Particularly, NIKON EPHIPHOT 200 OM, NIKON SMZ745 SM and ZEISS EVO SEM equipped with a Bruker energy-dispersive X-Ray spectrometer (EDX) were employed. The hardness was measured using a Vickers Affri Wiky 200JS digital instrument employing a 0.1 Kgf load for holding time equal to 15s (HV01/15), according to Vickers Hardness ISO 6507-1 (2018). For the evaluation of the stress concentration at the notch tip of the screw socket a FEM model using triangular plane elements with a linear formulation and axial symmetry option was employed [13-15]. Material has been assumed as linear elastic. Calculation has been made using the software Code Aster and two different geometric models.

Failure Analysis of the Connection Bolt

Visual analysis

Central bolt has been firstly removed from the driving shaft. In order to avoid possible damage of the fracture surface due to the disassembly, the shaft has been

circularly cut around the bolt facilitating its unscrewing. The central bolt is not rectilinear and appeared already permanently deformed before disassembly (Figure 5a), since it has been interested by a relevant plastic bending deformation before failure (Figure 5b). A sample of the base material to be used for metallographic analysis has been obtained from the central zone comprised between the fracture surface and the threaded connection.

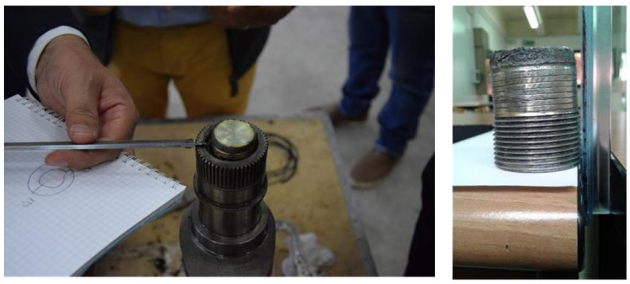

Figure 5: Central bolt a) before disassembly and b) after removal from engine shaft showing respectively eccentricity and bending.

Metallographic analysis

The microstructure of the bolt material after metallographic preparation and the chemical attack appears to be ferritic-pearlitic (Figure 6). The white grains are ferritic, the darker ones are perlitic (alternate lamellae of ferrite and cementite). The Vickers hardness measurements obtained by applying a load of 1 kgf for 15 seconds are uniform along the section (Figure 7) as well as the microstructure features. According to the state of art, the microstructure fits with the hardness values expected for the annealed CK45 [3-5,16].

Failure mechanism

Fracture surface corresponding to propeller side has been deeply examined by Stereomicroscopy (Figure 8) and Electron microscopy (Figure 9). The fracture surface of two diametrically opposite region highlighted in figure 8a are shown in figures 8b & 8c. The fracture surface in figure 8b appears flatter respect to the opposite zone, probably due to a dominant compressive stress state. The macroscopic analysis has not shown the presence in any point of fatigue crack propagation phenomenon [17-19].

Referring to the same regions in figure 8a, the fracture surfaces at the inner, medium, and external radius along the thickness have been analyzed by SEM (Figure 9). The fractures result mixed with both brittle and dimples areas. In particular, the absence of fatigue crack propagation regions on the fracture surface and the macroscopic plastic bending of the bolt (Figure 6) gives the indication that the failure was determined by a bending static overload [17-18,20-21], which determined firstly a plasticization of wide volume of material and finally the static failure.

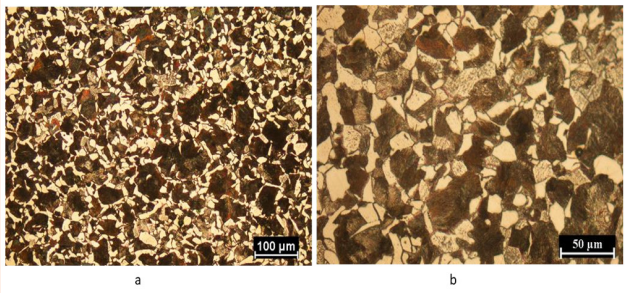

Figure 6: Optical microstructure of the bolt sample after Nital etching at a) 200X and b) 500X magnification showing ferritic (white) and darker perlitic phase (alternate lamellae of ferrite and cementite).

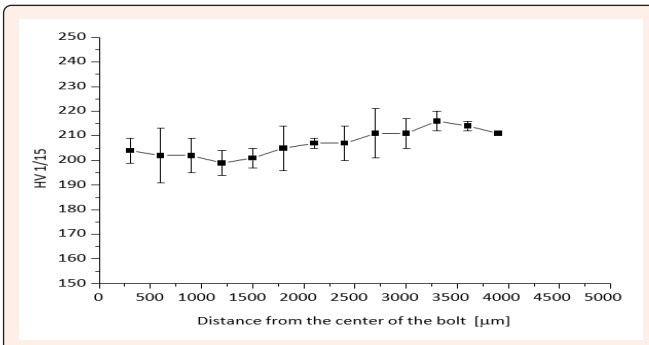

Figure 7: Vickers Hardness values from the center of the bolt along the radius.

The bolt failure was clearly originated by a static bending overload [17-18], as showed by the permanent deformation of the bolt, by the different macroscopic aspects of the diametrically opposite compressive and tensile zones, and by the mixed ductile/brittle fracture as generally happens in zone of severe stress concentration, corresponding to the sharp notch between bolt and hexagonal head.

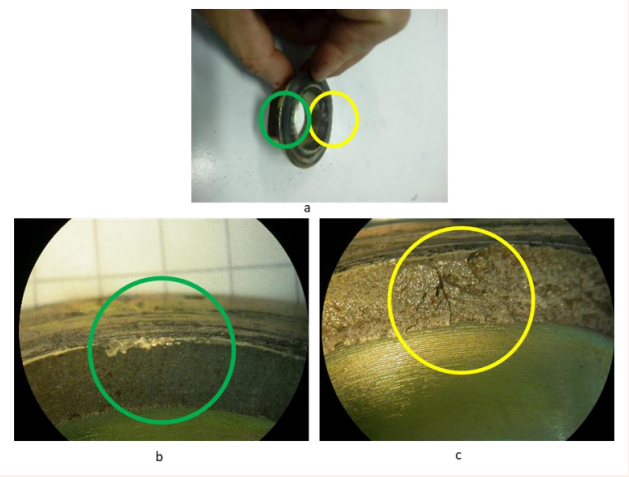

Figure 8: Macroscopic characterization of the fracture surface: a) yellow reference zone; b) diametral opposite zone

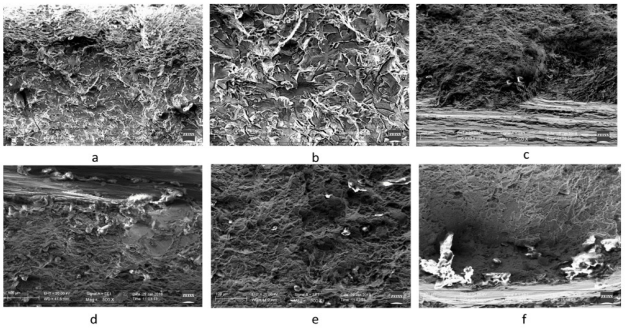

Figure 9: SEM fractographies of the reference zone (a, b, c) and diametral opposite zone (d, e, f) at the external radius (a, d) middle radius (b, e) and inner radius (c, f).

Failure analysis of the propeller hub

Visual analysis

After disassembling of the screwing holding of the broken blade (Figure 10), failure analysis has been concentrated on the screw socket and on the small part of blade end that has been retained by screw during failure (the part of the inner ring in figure 10). The original geometry of the socket is shown figure 11. All these components are made of 39NiCrMo3 steel and are mounted together using the M52x2 screw. Failure occurred in correspondence of the notch between the two cylindrical features having diameters of 60 and 82mm. In figure 11 the notch is characterized by a tip radius of 1mm.

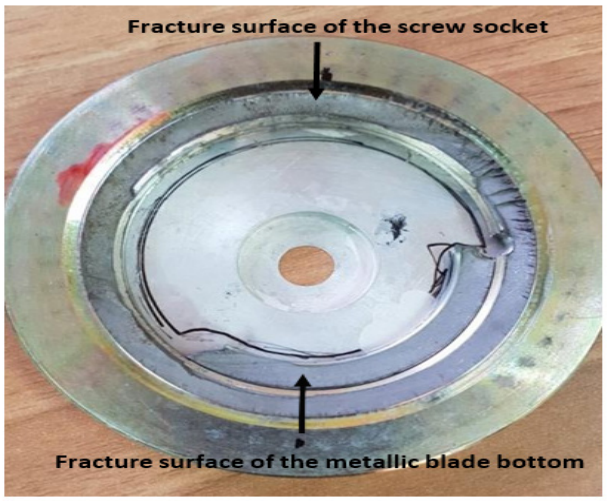

Figure 10: Fracture surface of the screw socket (external zone) and of the part of blade bottom that has been retained by screw during failure (inner zone).

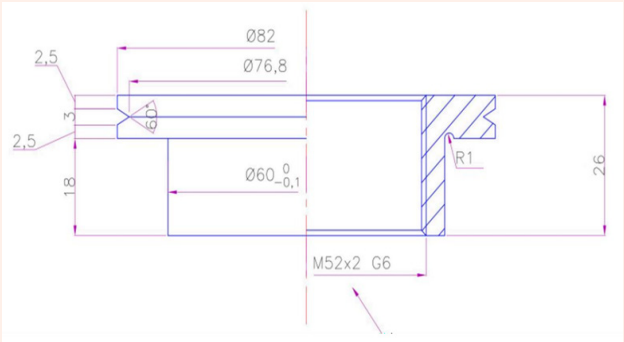

Figure 11: Geometry of the screw socket

Metallographic analysis

The microstructure of the screw socket sample after metallographic preparation and the Nital chemical attack exhibits tempered martensite (Figure 12). Nichel, in combination with Chromium, improves the hardenability delaying both the austenite to perlite and austenite to bainite transformations. So, oil quenching is employed to produce a martensitic structure from austenitizing temperature (850°C) [3-5]. The further addition of 0.2% Mo increases still more hardenability and minimizes the susceptibility to embrittlement during the tempering step. The average value of Vickers hardness measurements was found equal to 304±3. Microstructural features and hardness are compatible with those of a 39NicrMo3 oil quenched and tempered at 650°C [3,4].

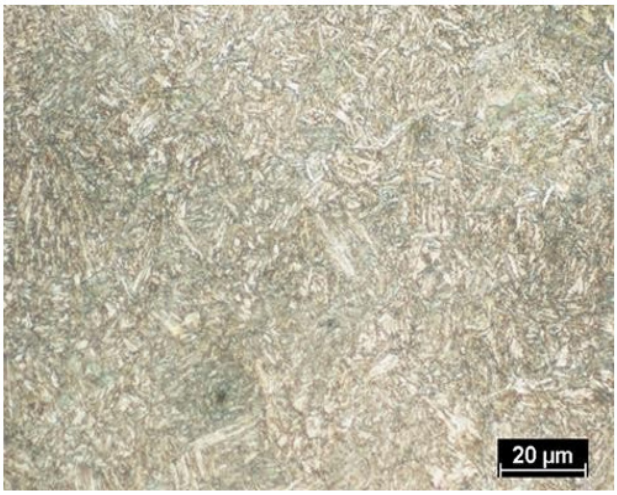

Figure 12: Optical micrograph of the screw socket sample showing tempered martensitic microstructure

Failure mechanism

The surface failure of the screw socket is a classic fatigue failure determined by alternating plane bending [16-17, 20-21]. Fatigue cracks initiated in correspondence of opposite region of the fillet radius of the notch and propagated for a wide extension in the screw socket. Starting from several initiation points located on the external radius and in opposite regions with respect to the neutral axis of the bending load, cracks propagate firstly radially towards the centre of the socket and then circumferentially, as highlighted in figure 13. This is particular evident at the blade bottom (inner area in figure 10 & 13a), where it is possible to identify the classical fatigue striations perpendicular to the crack propagation front (Figure 13b). So, that propagation passed through the screw and also interested the blade bottom. At the moment of the final failure, the partial zone of the blade end was retained by the screwing and it has been found attached at the failed socket. The two propagating zones are symmetrically disposed about the ideal axis reported in yellow (Figure 13a), which represents approximatively the neutral axis of the fatigue bending loads. The region around the neutral axis in the blue circle of figure 13a corresponds to the brittle final failure due to the insufficient section needed to hold the centrifugal load.

Many regions of fatigue striations have been recognized (Figure 14b) through a SEM analysis of the fracture zone highlights by the red circle of figure 14a. At higher magnification (Figure 14c), the surface between striations appears smoothed as expected in regions where fatigue propagation has occurred. Moreover, in the opposite side of the fracture surface, highlighted with blue circle (Figure 14d), a relevant number of microcracks, characteristic of the fatigue initiation phase, has been observed (Figure 14e).

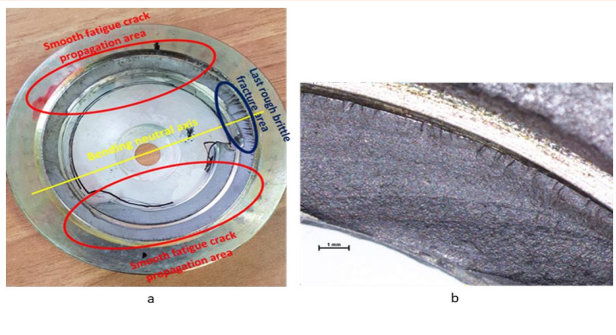

Figure 13: Identification of the typical area produced by fatigue failure determined by plane bending (a) and fatigue striations at the blade bottom area (b).

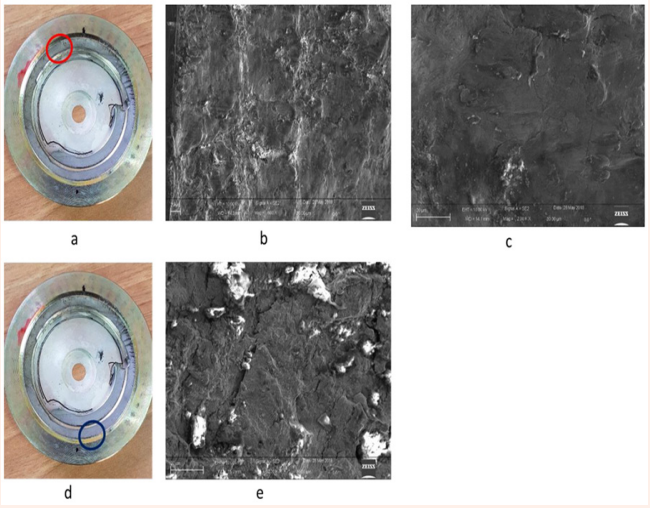

Figure 14: SEM analysis of the fracture surface highlight in the red circle (a) exhibiting fatigue striation observed at different magnification: 500X (b) and 2000X (c). In the blue circle (d) fracture surface exhibits fatigue striations together with microcrack (e).

So, according to the previous analysis, the failure was determined by a bending plane fatigue loading that has been enhanced by the stress concentration at the notch tip present in the screw socket. Crack initiated at the notch and rapidly propagated firstly radially and then circumferentially up to the section had become insufficient to hold the tensile centrifugal load, determining the final brittle failure of the screw socket (blue circle in figure 13a), and the loss of the blade.

Analysis of the Notch in the Unbroken Blade

The visual examination of the notch in the screw socket of the unbroken blade showed unequivocally the presence of an extended circumferential crack. The circumferential crack has been shown in figure 15, as a sequence of pictures taken in correspondence of the four quadrants, in which has been ideally divided the circumferential notch. Fixing an arbitrary direction as 0°, corresponding to the localization of the cord of the blade profile, the crack seems particularly marked in the quadrants comprises between 0°-90° and 180°-270°, while crack is absent between 90°-135° and 270°-315°. The localization of the cracks is coherent with the localization of the nucleation and propagation zones of the fracture surface of figures 13 & 14. The previous features can be better observed by stereomicroscope analysis (Figure 16). The entity of the notch crack preludes to an imminent final failure. So, the process failure of the second blade has been interrupted just by the failure of the first one.

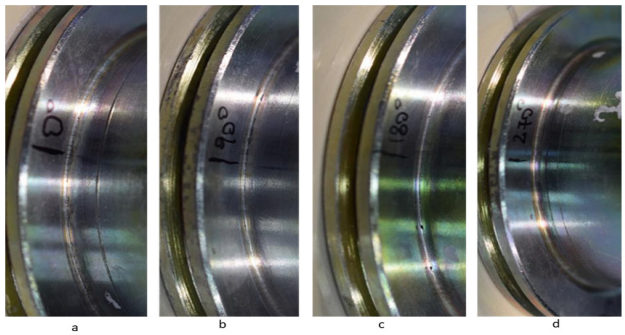

Figure 15: Circumferential examination of the screw socket notch from different points of view: a) 0°; b) 90°; c) 180°; d) 270°

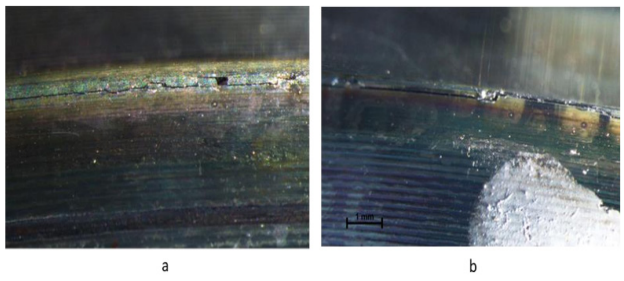

Figure 16: Particular of circumferential lack of materials (a) and crack opening (b).

Identification of Probable Causes of Failure

The loads acting on the blade during flight are both centrifugal (due to the rotation of the propeller) and aerodynamic (generated by the motion of the aerodynamic profile). The first one is essentially a tensile load which is statically applied. It is constant at a fixed rotation speed but, anyway, changes slowly. On the other hand, the aerodynamic load acts transversally with respect to the blade and are characterized by fluctuations depending by changing of aerodynamic condition. This load could be considered as a diffused bending load that is also affected by the orientation of the blade with the respect of the streamline motion. The interaction of the aerodynamic load with the natural bending frequency of the blade could impose narrow vibration and oscillation of the stress state. So, the blade root is subjected to a relevant axial stress and quite limited fatigue load induced by fluctuating bending loads acting on the blade. The variable stresses are usually so narrow that can be neglected, and the blade root can be structurally verified considering just the centrifugal load. But not in the case of this study. In fact, the fatigue failure of the blade, and the imminent failure of the unbroken one, demonstrated that the stress amplitude induced by plane bending at the root of the blade was relevant. Consequently, the local stress state in the failure zone was analyzed to establish the cause of the failure. Local stress state in the region of the notch is highly depending by the applied load and by notch geometry, in particular the radius at the notch tip.

The measurement of the radius of the notch tip has been carried out on the unbroken blade by making a calk of the notch in silicon past (Figure 17a). A representative section of the notch section was therefore obtained and compared with a radius measurement instrument for tips (Figure 17b). As evident, the geometry of the notch is deeply different from the nominal one reported in figure 11 and equal to 1mm. Moreover, the silicon calk has also detected the presence of a significant undercut surface that reduces the net section of the screw socket (Figure 17b). Finally, the notch radius was proven to be equal to 0.5mm by drawing the two red circles in figure 17b having a radius of 0.5 and 1mm, respectively. The stress concentration due to the actual value of notch radius has been analysed by a FEM model based on Code Aster software and compared with the nominal one.

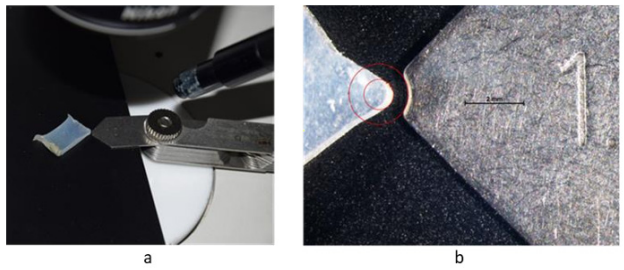

Figure 17: Notch radius evaluation: a) particular of the calk; b) evaluation per comparison using a radius measurement instruments for tips and two superimposed cad circles.

Since the aim is to evaluate the increase of the stress concentration due to the reduction of the notch tip, a simple axial load was considered. Assuming this condition, it is possible to exploit the axial symmetry of the component and of the applied load to build a FEM model using triangular plane elements with a linear formulation and axial symmetry option. Material has been assumed as linear elastic. Model A (notch radius of 1mm) and Model B (notch radius of 0.5mm) are shown in figure 18. The same figure reported the loading condition that was applied: the bottom of the component model was fixed in the vertical direction and a uniform load was applied on the annulus of the screw socket. It is worth to note that, by neglecting the presence of the undercut highlighted by silicon calk, the effective stress concentration at the notch tip results underestimated.

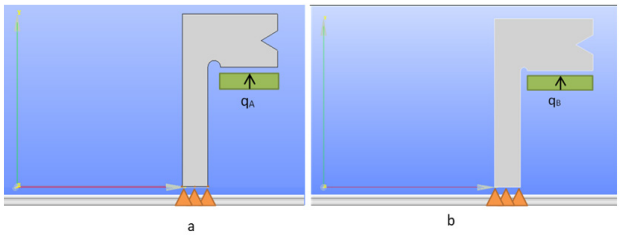

Figure 18: Geometry and load condition of the FEM models for a) Model A notch radius r = 1mm and b) Model B notch radius r = 0,5 mm.

For a direct comparison of the effect of the notch geometry on the stress concentration, the same distributed load must be applied to the two models. As the values of notch radius modify the areas, on which the load is applied, as in the following:

$$S_A = \frac{\pi}{4}(D^2 - (d+4r)^2) = \frac{\pi}{4}(82^2 - (60+4)^2) = 2064mm^2 \quad (1)$$

$$S_B = \frac{\pi}{4}(D^2 - (d+4r)^2) = \frac{\pi}{4}(82^2 - (60+2)^2) = 2261mm^2 \quad (2)$$

a unitary load on the surface of model A $q_A = 1\ N/mm^2$ determines that the same load condition is obtained on the model B applying a distributed load q_B opportunely scaled:

$$q_B = q_A \frac{S_A}{S_B} = 0.9125N/mm^2 \quad (3)$$

The FEM results showed that the stress state at the notch radius is characterized by relevant stress both in radial and axial direction. The radial stress (SXX), axial stress (SYY) and the Von Mises equivalent stress (SVM) are shown and compared in figure 19. The peak stresses are resumed in table 1, in which also the percentage increase of the stress component of model B with respect to the model A is reported.

Table 1: Comparison of maximum stress component of models A and B.

	model A – r = 1mm	model B – r = 0.5mm	var. %
S_{XX} [N/mm²]	19.38	25.88	+33%
S_{YY} [N/mm²]	30.92	33.83	+9.40%
S_{VM} [N/mm²]	29.95	35.09	+17.20%

As showed by results in table 1, all the stress component increased in model B. Particularly, radial stress suffers an increase of 33% of the stress concentration. That increasing in the notch stress concentration (33% in table 1) is very significant although it has been underestimated by having neglected the presence of the undercut. Therefore, the smaller value of the notch radius equal to 0,5mm has to be responsible for the fatigue failure of the screw socket.

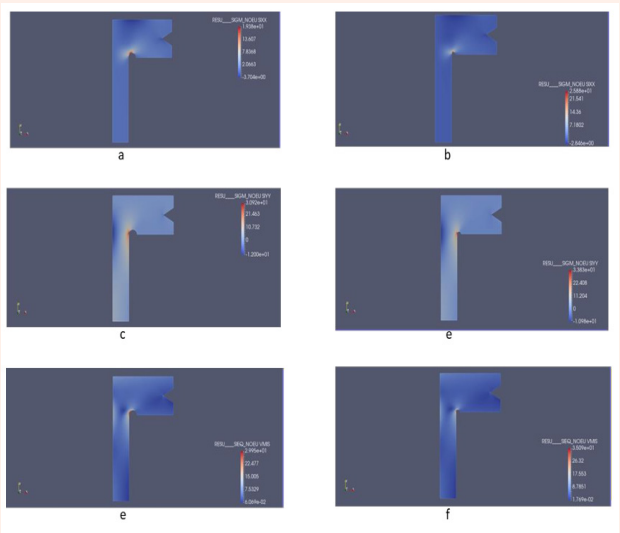

Figure 19: Comparison of the stress state for Model A notch radius r = 1 mm (a, c, e) and Model B notch radius r = 0,5 mm (b, d, f): Radial stress XXS (a, b), axial stress YYS (c, d), equivalent Von Mises stress VMS (e, f).

Conclusion

The mechanical and microstructural analysis of the connection bolt and screw socket that were found broken after the aircraft crash allowed to define the causes of the accident, as briefly resumed in the following:

a) The microstructure and metallurgical analysis the CK45 bolt and the 39 NiCrMo3 screw socket did not show any defects or anomalies in the parts, both in microstructure and mechanical behaviour.

b) The connection bolt fracture surfaces were found mixed (ductile and brittle) and the relevant macroscopic permanent deformation of the component was due to a bending overload.

c) The screw socket fracture surfaces clearly showed the presence of fatigue cracks initiation and propagation. Failure surface was characterized by two large propagation zones symmetrically disposed with respect to a diametral axis and at least one zone of brittle fracture in the last residual section. Failure was found induced by the application of an alternate plane bending stress in presence of a relevant axial mean stress.

d) The visual examination of the unbroken blade showed the presence of cracks nucleated on the notch of the screw socket, which failure was imminent.

e) The fatigue process on the two screw sockets was due to a critical stress state at the notch tip, induced by an unsuitable notch radius, lower than the designed one.

f) The failure investigation confirmed the catastrophic effect that a minimum difference of 0.5 mm in a critical notch radius could have in the structural integrity of a component. Moreover, the analysis has clarified the accident dynamics, establishing that the primary failure occurred between the blade and the propeller, followed by the failure of the bolt connecting the propeller to the engine shaft.

References

1. Brooks CR, Choudhury A (2002) Failure Analysis of Engineering Materials. In: 1st Edition, McGraw-Hill Education.
2. Clifford M (1998) A Practical Guide to Engineering Failure Investigation. Professional Engineering Publishing Limited.
3. Llewellyn D, Hudd R (1998) Steels: Metallurgy and applications. In: Elsevier, Butterworth-Heinemann.
4. Smith WF (1993) Structure and Properties of Engineering Alloys. In: 2nd Edition, McGraw-Hill.
5. Bhadeshia HKDH, Honeycombe R (2006) Steels: microstructure and properties. Butterworth- Heinemann.
6. Langari J, Aliakbari K, Nejad RM, Abbasnia SK (2023) Failure analysis of CK45 steel crankshaft in light truck diesel engine. Engineering Failure Analysis pp. 145.
7. Yousefi M, Rajabi M, Kerahroodi A (2021) Graphitization cracks in CK45 steel clips of turbofans. Engineering Failure Analysis pp. 125.
8. Galedari SA, Khoei SMM (2013) Effect of pulse frequency on microstructure and surface properties of Ck45 steel treated by plasma electrolysis method. J Alloys Compd 551: 415-421.
9. Firrao D, Matteis P, De Sario A (2021) Low temperature tempering of low alloy 39NiCrMo3 and 36NiCrMo16 quenched and tempered steels. Mat Design Process Comm 3(1): 142.
10. Campagnolo A, Dabalà M, Meneghetti G (2019) Effect of Salt Bath Nitrocarburizing and Post-Oxidation on Static and Fatigue Behaviours of a Construction Steel Metal 9(12): 1306.
11. Spezzapria M, Settimi AG, Pezzato L, Novella MF, Forzan M, et al. (2017) Effect of prior microstructure and heating rate on the austenitization kinetics of 39NiCrMo3 Steel. Steel Research International 88(5).
12. Speidel A, Lutey AHA, Mitchell SJ, Rance GA, Liverani E, et al. (2016) Surface modification of mild steel using a combination of laser and electrochemical processes. Surface & Coatings Technology 307: 849-860.
13. Cook RD, Malkus DS, Plesha ME, Witt RJ (2002) Concepts and Applications of Finite Element Analysis. In: 4th edition, John Wiley & Sons, Inc.
14. Pilkey WD, Pilkey DF (2008) Peterson's Stress Concentration Factors. In: 3rd Edition, John Wiley & Sons, Inc.
15. Murakami Y (2017) Theory of Elasticity and Stress Concentration. John Wiley & Sons, Inc.
16. Magdeski JS, Slavkov DS, Cvetkovski ST (2003) Effects of heat treatment on the mechanical and microstructural properties of improvable steel C. In: Macedonia R ,1531, Proceedings of 3rd BMC--Ohrid.
17. (1987) ASM Metal handbook: Fractography, Metals Park, Ohio: American Society for Metals, 12.
18. Mullen MJ, Griebel AH, Tartaglia JM (2007) Fracture surface analysis. Advanced materials & processes.
19. Smith RA, Miller KJ (1977) Fatigue cracks at notches. Int J Mech Sci 19: 11-22.
20. Hou N, Ding N, Qu S, Guo W, Liu L, et al. (2022) Failure modes, mechanisms and causes of shafts in mechanical equipment. Engineering Failure Analysis 136.
21. Bonnen JJF, Topper TH (1999) The effect of bending overloads on torsional fatigue in normalized 1045 steel. International Journal of Fatigue 21(1): 23-33.